2013 IEEE/RSJ International Conference on
Intelligent Robots and Systems (IROS)
November 3-7, 2013. Tokyo, Japan

Visual Servo Control of Cable-driven Soft Robotic Manipulator

Hesheng Wang, *Member, IEEE*, Weidong Chen, *Member, IEEE*, Xiaojin Yu, Tao Deng, Xiaozhou Wang and Rolf Pfeifer

***Abstract*—Aim at enhancing dexterous and safe operation in unstructured environment, a cable-driven soft robotic manipulator is designed in this paper. Due to soft material it made of and nearly infinite degree of freedom it owns, the soft robotic manipulator has higher security and dexterity than traditional rigid-link manipulator, which make it suitable to perform tasks in complex environments that is narrow, confined and unstructured. Though the soft robotic manipulator possesses advantages above, it is not an easy thing for it to achieve precise position control. In order to solve this problem, a kinematic model based on piecewise constant curvature hypothesis is proposed. Through building up three spaces and two mappings, the relationship between the length variables of 4 cables and the position and orientation of the soft robotic manipulator end-effector is obtained. Afterwards, a depth-independent image Jacobian matrix is introduced and an image-based visual servo controller is presented. Applied by adaptive algorithm, the controller could estimate unknown position of the feature point online, and then Lyapunov theory is used to prove the stability of the proposed controller. At last, experiments are conducted to demonstrate rationality and validity of the kinematic model and adaptive visual servo controller.**

I. Introduction

Because of its additional advantages over rigid robots, discrete hyper-redundant robots and hard continuum robots, such as infinite number of DOF, high safety and dexterity, ability to work in both structured and unstructured environment, soft robots have been studied by researchers recently [1]-[2]. Soft robots are often inspired by a biological structure of animals called muscular hydrostats, which can be found in mammal tongues, elephant trunks [3]-[4] and octopus tentacles [5]-[6] etc. One interesting properties of these robot is that they have redundant DOF, which make them could achieve complicated task even in crowded environment, such as search and rescue tasks [7], surgical applications [8] -[9] and so on.

Although soft robots have many potential advantages, they also encounter a series of problems: how to establish the kinematic and dynamic models of soft robots and how to control the soft robots to perform complex tasks which need precise position control. Hannan et al. [10] presented a kinematic model for the Elephant Trunk Manipulator and other continuum style robots. Webster et al. [11] reviewed recent kinematic modeling results for constant curvature continuum robotics. Haddadin et al. [12] designed a 2 DOF continuum type robot – the Tubot and developed analytical and experimental kinematics to improve safety of the robotic manipulator under uncontrolled impacts. Zheng et al. [13] presented a 3D dynamic model of an octopus like arm. This continuum robot is composed of a multi-segment structure. Camarillo et al. [14] developed a new linear kinematic model for tendon-driven continuum manipulators. The methods provided in [10]-[12] cannot be applied directly to motion control for not taking nonlinear, large deformation and gravitation effects into account, whereas the methods provided in [13]-[14] are too costly to be real-time implemented. Besides, the methods mentioned above are aim to cope with the cases that the shape of the soft robotic manipulator must be a cylinder, which might be not applied to our cone-shaped manipulator.

To control the motion of soft robots, many sensors are involved. Among them, vision system is a promising way for soft robots to achieve precise motion control. Visual servoing has been extensively studied over last decades and many approaches have been proposed such as homography method in [15]. In our earlier work [16]-[18], a visual servoing method was developed based on the concept of depth-independent interaction matrix. Since the soft robots have different kinematic and dynamic behaviors compared with rigid robots, it is worth to develop a visual servoing algorithm for soft robots. To the best of our knowledge, there is no literature indicates that visual servoing has been introduced into the motion control of soft robots.

In this paper, a soft robotic manipulator inspired by octopus is designed and fabricated. A kinematic model with the concept of piecewise constant curvature is presented to build up the relationship between the length variables of the cables and the position and orientation of the end-effector of the soft robotic manipulator. A kinematics-based adaptive controller for image-based visual servoing is developed to decrease the errors of the feature point on image plane, and control the end-effector of soft robotic manipulator to move to the desired

* This work was supported in part by Specialized Research Fund for the Doctoral Program of Higher Education of China under Grants 20100073120020 and 20100073110018, in part by Shanghai Municipal Natural Science Foundation under Grant 11ZR1418400, in part by the Natural Science Foundation of China under Projects 61105095, in part by China Domestic Research Project for the International Thermonuclear Experimental Reactor (ITER) under Grant 2012GB102001, in part by Medical Engineering Project of Shanghai Jiao Tong University under Grant YG2011ZD08.

Hesheng Wang, Weidong Chen, Xiaojin Yu and Tao Deng are with the Department of Automation, Shanghai Jiao Tong University, and Key Laboratory of System Control and Information Processing, Ministry of Education of China, Shanghai 200240, China (e-mail: wdchen@sjtu.edu.cn; wanghesheng@sjtu.edu.cn).

Xiaozhou Wang is with Shanghai Chest Hospital, Shanghai Jiao Tong University, Shanghai, china.

Rolf Pfeifer is with Artificial Intelligence Laboratory, Department of Informatics, University of Zurich , Andreasstrasse 15 (Office 2.32), 8050 Zurich, Switzerland (e-mail: pfeifer@ifi.uzh.ch).

position. The controller is based on the depth-independent interaction matrix. It is then possible to estimate the unknown 3D coordinate of the feature point by an adaptive algorithm. The asymptotic stability of the proposed controller is proved by the Lyapunov theory. Experiments on the soft robotic manipulator have been conducted to verify the performance of this controller.

II. DESIGN CONCEPT

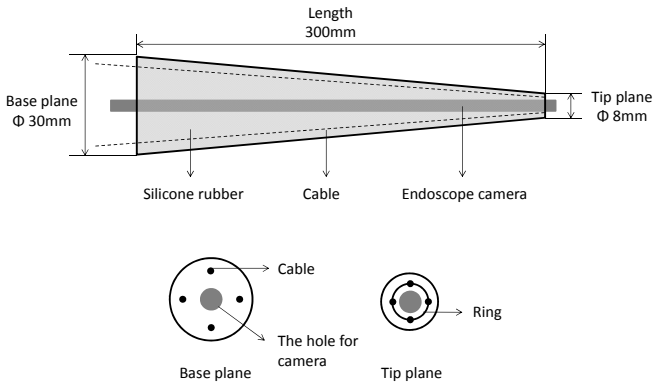

Fig.1 The cable-driven soft robotic manipulator.

To perform dexterous and safe operation in complex environments, "soft" characteristic is an essential cue for the robotic manipulator. As shown in Fig.1, the soft robotic manipulator developed in our laboratory is made of silicone rubber and has no rigid structure inside. Inspired by octopus tentacle, the current prototype is cone-shaped, and 300mm in length, 8mm and 30mm in diameters of the tip plane and the base plane respectively. In order to decrease the manipulator size, the actuation system which consists of servomotors and pulleys is apart from soft robotic manipulator. Instead, 4 cables are uniform distributed near the outer surface of the manipulator and run through the whole body length to connect the soft robotic manipulator and the peripheral actuation system. One side of the cables is tied to a small ring embedded in the tip, and the other side is coined around pulleys. In addition, an endoscope camera is embedded along the center axis to provide visual feedback for the controller to regulate the end-effector of the soft robotic manipulator moving to desired position and orientation.

III. KINEMATIC MODEL

The soft robotic manipulator has no links and joints, and the position and orientation of the end-effector of the soft robotic manipulator is controlled by 4 cables. To derive the relationship between the length variables of 4 cables and the position and orientation of the end-effector, three spaces (namely actuation space, virtual joint space and task space) and two mappings (namely actuation space - virtual joint space mapping and virtual joint space - task space mapping) are set up. Let q be the length variables of 4 cables in the actuation space and p be the position and orientation of the end-effector in the task space. The configuration of the soft robotic manipulator is expressed by the virtual joint variables ϕ,θ,r . Specifically, ϕ denotes the angle between the bending plane and the positive direction of x axis, θ and r denote the curvature angle and curvature radius of the bending plane respectively.

The soft robotic manipulator is cone-shaped, thus the central axis varies in curvature according to the radius of transverse section. To simplify the solving procedure, the piecewise constant curvature hypothesis is introduced, that is, evenly dividing the whole body of the soft robotic manipulator into n segments, and each segment can be treated as a cylinder that the radius of the upper section is equal to the one of the lower section.

A. Actuation space - virtual joint space mapping

Fig.2 illustrates the i-th segment of the soft robotic manipulator. Let O_{i-1} and O_i be the center of the upper section and lower section respectively, then establish rectangular coordinate frames $O_{i-1}-x_{i-1}y_{i-1}z_{i-1}$ and $O_i-x_iy_iz_i$, in which the positive direction of x axis is from O to cable 1 and the positive direction of y axis is from O to cable 2, thus z axis can be decided by right-hand rule.

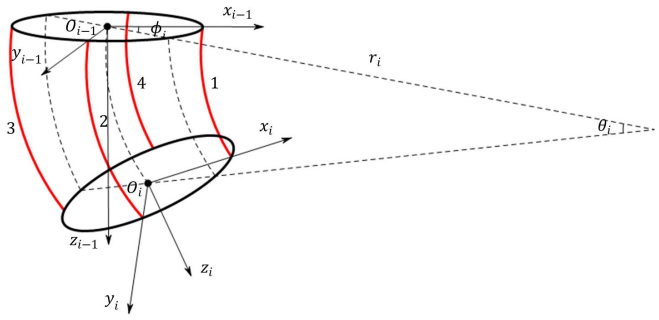

Fig.2 The i-th segment of the soft robotic manipulator.

Let L be the initial length of 4 cables and q_1,q_2,q_3,q_4 be the length variables of 4 cables, the current lengths of 4 cables l_1,l_2,l_3,l_4 can be represented as:

$$\begin{aligned} l_1 &= L-q_1 \\ l_2 &= L-q_2 \\ l_3 &= L-q_3 \\ l_4 &= L-q_4 \end{aligned} \tag{1}$$

The current length of the central axis l can be represented as:

$$l=\frac{l_1+l_2+l_3+l_4}{4} \tag{2}$$

Because the soft robotic manipulator is divided into n segments, the current length of 4 cables and the central axis of the i-th segment can be denoted by $\frac{l_1}{n},\frac{l_2}{n},\frac{l_3}{n},\frac{l_4}{n}$ and $\frac{l}{n}$.

Let R_1 and R_2 be the radiuses of the base plane and tip plane, where $R_2>R_1$, the radius of transverse section of the i-th segment R_i can be represented as:

$$R_i=R_2+\frac{i}{n}\left(R_1-R_2\right) \tag{3}$$

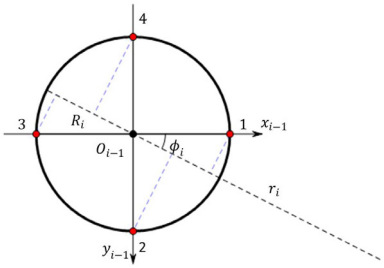

Fig.3 The top view of the the upper section.

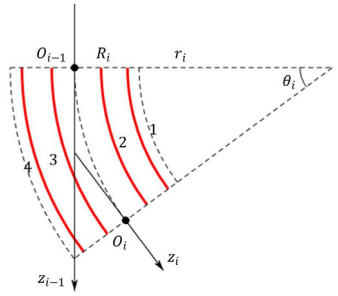

Fig.4 The cutaway view of the bending plane.

From the top view of the upper section shown in Fig.3 and the cutaway view of the bending plane shown in Fig.4, it is not difficult to derive the geometrical relationship between the virtual joint variables of the i-th segment ϕ_i, θ_i, r_i and the current length of 4 cables of the i-th segment $\frac{l_1}{n}, \frac{l_2}{n}, \frac{l_3}{n}, \frac{l_4}{n}$, which can be written as:

$$\begin{aligned} \frac{l_1}{n} &= \theta_i \left(r_i - R_i \cos\phi_i \right) \\ \frac{l_2}{n} &= \theta_i \left(r_i - R_i \sin\phi_i \right) \\ \frac{l_3}{n} &= \theta_i \left(r_i + R_i \cos\phi_i \right) \\ \frac{l_4}{n} &= \theta_i \left(r_i + R_i \sin\phi_i \right) \end{aligned} \tag{4}$$

Substitute Eq. (1) into Eq. (4) and simplify it, the virtual joint variables of the i-th segment ϕ_i, θ_i, r_i can be written as following form:

$$\phi_i = \tan^{-1} \frac{q_4 - q_2}{q_3 - q_1} \tag{5}$$

$$\theta_i = \frac{\sqrt{\left(q_3 - q_1\right)^2 + \left(q_4 - q_2\right)^2}}{2nR_i} \tag{6}$$

$$r_i = \frac{2\left(L - q\right)R_i}{\sqrt{\left(q_3 - q_1\right)^2 + \left(q_4 - q_2\right)^2}} \tag{7}$$

where q in Eq. (7) can be represented as:

$$q = \frac{q_1 + q_2 + q_3 + q_4}{4} \tag{8}$$

By Eq. (5) - Eq. (7), the mapping from actuation space to virtual joint space, that is, the relationship between the length variables of 4 cables q_1, q_2, q_3, q_4 and the virtual joint variables of the i-th segment ϕ_i, θ_i, r_i is obtained.

B. Virtual joint space - task space mapping

In classical kinematics analysis of rigid-link manipulator, the Denavit-Hartenberg method (D-H method) is a universal way to derive the relationship between the joint variables and the position and orientation of the end-effector. Although the soft robotic manipulator has no links and joints, the D-H method can be extended to compute the mapping from virtual joint space to task space. As shown in Fig.5, the homogeneous transformation from the coordinate frames of the upper section to the coordinate frames of the lower section can be treated as the result of performing a series of translation and rotation in order. According to the definition of the parameters in the D-H method, the translation and rotation described above can be listed a table as follows:

Table.1 The D-H method parameters list.

Order	ϑ	d	a	α
1	ϕ_i	0	0	$-\pi/2$
2	$\theta_i/2$	0	0	$\pi/2$
3	0	$2r_i \sin(\theta_i/2)$	0	$-\pi/2$
4	$\theta_i/2$	0	0	$\pi/2$
5	$-\phi_i$	0	0	0

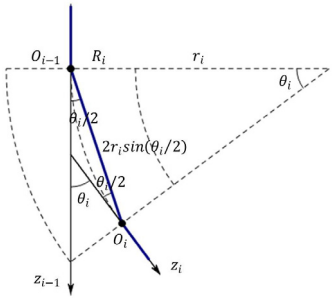

Fig.5 The translation and rotation of the i-th segment.

Thus the homogeneous transformation matrix between the upper section and lower section of the i-th segment ${}^{i-1}T_i$ can be represented as:

$${}^{i-1}T_i = \begin{bmatrix} c^2\phi_i\left(c\theta_i - 1\right) + 1 & s\phi_i c\phi_i\left(c\theta_i - 1\right) & c\phi_i s\theta_i & r_i c\phi_i\left(1 - c\phi_i\right) \\ s\phi_i c\phi_i\left(c\theta_i - 1\right) & s^2\phi_i\left(c\theta_i - 1\right) + 1 & s\phi_i s\theta_i & r_i s\phi_i\left(1 - c\phi_i\right) \\ -c\phi_i s\theta_i & -s\phi_i s\theta_i & c\theta_i & r_i s\theta_i \\ 0 & 0 & 0 & 1 \end{bmatrix} \tag{9}$$

Apply chain rule to all of n segments, it is easy to gain the homogeneous transformation matrix between the base plane and tip plane, which can be written as:

$$T = {}^0T_1\,{}^1T_2 \cdots {}^{n-1}T_n \tag{10}$$

Let v and w be the line velocity and angular velocity of end-effector respectively, and $\dot{q}$ be the velocities of 4 cables. Based on the direct kinematics analysis above, the differential kinematics of the soft robotic manipulator can be represented as follows:

$$\begin{bmatrix} v \\ w \end{bmatrix} = J(q)\dot{q} \tag{11}$$

where $J(q)$ in Eq. (11) represents 6×4 Jacobian matrix.

IV. Visual Servo Control

A. Perspective projection model

In order to implement image-based visual servo control, perspective projection model should be built up firstly. As shown in Fig.6, an eye-in-hand system of the soft robotic manipulator is set up. Define three coordinate frames, namely the base frame, the end-effector frame and the camera frame. Let ${}^{e}T_{b}(q(t))$ be the homogeneous transformation matrix of the base frame with respect to the end-effector frame, it can be computed by direct kinematics of the soft robotic manipulator and has relation to the length variables of 4 cables $q(t)$. Let ${}^{c}T_{e}$ be the homogeneous transformation matrix of the end-effector frame with respect to the camera frame, it is independent of the length variables of 4 cables $q(t)$ for the relative position between the endoscope camera and the end-effector is constant.

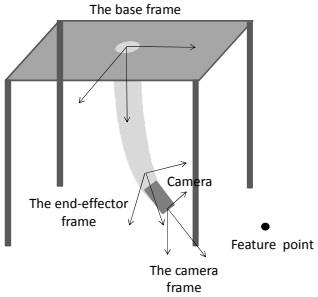

Fig.6 The eye-in-hand system of the soft robotic manipulator.

Introduce a feature point fixed in 3D space. Let ${}^{b}x$, ${}^{e}x(t)$ and ${}^{c}x(t)$ be 3D coordinates in the base frame, the end-effector frame and the camera frame respectively, in which ${}^{b}x$ is unknown. Thus the coordinates of the feature point in the end-effector frame and the camera frame can be written in homogeneous coordinate forms as follows:

$$\begin{bmatrix} {}^{e}x(t) \\ 1 \end{bmatrix} = {}^{e}T_{b}(q(t)) \begin{bmatrix} {}^{b}x \\ 1 \end{bmatrix} \tag{12}$$

$$\begin{bmatrix} {}^{c}x(t) \\ 1 \end{bmatrix} = {}^{c}T_{e} \begin{bmatrix} {}^{e}x(t) \\ 1 \end{bmatrix} \tag{13}$$

Assume that the endoscope camera is a pin-hole camera, and it satisfies the imaging principles of perspective projection. Denote the 2D coordinate of the feature point on the image plane by $y(q(t))$ and the depth of the feature point in the camera frame by $z(q(t))$, therefore the projection of the feature point on the image plane also can be written in homogeneous coordinate forms:

$$\begin{bmatrix} y(q(t)) \\ 1 \end{bmatrix} = \frac{1}{z(q(t))} M \begin{bmatrix} {}^{e}x(t) \\ 1 \end{bmatrix} \tag{14}$$

where M is called perspective projection matrix. Rewrite Eq. (14), $y(q(t))$ and the depth $z(q(t))$ can be represented as:

$$y(q(t)) = \frac{1}{z(q(t))} P \begin{bmatrix} {}^{e}x(t) \\ 1 \end{bmatrix} \tag{15}$$

$$z(q(t)) = m_3^{T} \begin{bmatrix} {}^{e}x(t) \\ 1 \end{bmatrix} \tag{16}$$

where $P = \begin{bmatrix} m_1^{T} & m_2^{T} \end{bmatrix}^{T}$, in which $m_i^{T}\ (i = 1,2,3)$ denotes the i-th row vector of the perspective projection matrix M.

Differentiate Eq. (15) - (16), the 2D velocity of the feature point on the image plane $\dot{y}(q(t))$ and the change rate of the depth in the camera frame $\dot{z}(q(t))$ can be described as:

$$\dot{y}(q(t)) = \frac{1}{z(q(t))} A(y(t), q(t)) \begin{bmatrix} v(t) \\ w(t) \end{bmatrix} \tag{17}$$

$$\dot{z}(q(t)) = b(q(t)) \begin{bmatrix} v(t) \\ w(t) \end{bmatrix} \tag{18}$$

where $A(y(t), q(t))$ is called depth-independent image Jacobian matrix. $A(y(t), q(t))$ and $b(q(t))$ can be written in concrete forms as follows:

$$A(y(t), q(t)) = \left(P - y(t) m_3^{T}\right) \begin{bmatrix} -I_{3\times 3} & skew({}^{e}R_{b}(q(t)) {}^{b}x + {}^{e}p_{b}(q(t))) \\ 0_{1\times 3} & 0_{1\times 3} \end{bmatrix} \begin{bmatrix} {}^{e}R_{b}(q(t)) & 0 \\ 0 & {}^{e}R_{b}(q(t)) \end{bmatrix} \tag{19}$$

$$b(q(t)) = m_3^{T} \begin{bmatrix} -I_{3\times 3} & skew({}^{e}R_{b}(q(t)) {}^{b}x + {}^{e}p_{b}(q(t))) \\ 0_{1\times 3} & 0_{1\times 3} \end{bmatrix} \begin{bmatrix} {}^{e}R_{b}(q(t)) & 0 \\ 0 & {}^{e}R_{b}(q(t)) \end{bmatrix} \tag{20}$$

where ${}^{e}R_{b}(q(t))$ and ${}^{e}p_{b}(q(t))$ denote the rotation matrix and translation vector of the base frame with respect to the end-effector frame.

B. Adaptive Controller Design

To regulate the end-effector of the soft robotic manipulator, we place the end-effector in a desired position in 3D space using teaching method and then record the 2D coordinate of the feature point on the image plane. The control task of image-based visual servoing is comparing the current position and desired position of the feature point and using position error to generate control signal, and the task is finished when the position error to be zero.

To design an image-based visual servo controller, the key point is to estimate the unknown position of the feature point in the base frame. With regards to this, an adaptive controller is presented to estimate the unknown position of the feature point online. To simplify the analytic process, we only take one feature point into account, while the controller also can be applied to the situation that consists of several feature points.

Let $y(t)$ and y_d be the current position and desired position of the feature point on the image plane respectively, the position error $\Delta y(t)$ can be written as:

$$\Delta y(t) = y(t) - y_d \tag{21}$$

Based on the method of PD feedback control with gravity compensation, a kinematics-based visual servo controller is designed as follows:

$$\begin{aligned}\dot{q}(t) = &-J^T(q(t))\hat{A}^T(y(t),q(t))K_1\Delta y(t)\\ &-\frac{1}{2}J^T(q(t))\hat{b}^T(q(t))\Delta y^T(t)K_1\Delta y(t)\end{aligned} \tag{22}$$

in which the left side $\dot{q}(t)$ in Eq. (22) represents the velocities of 4 cables. The first item in the right side represents image feedback, and the estimate value of the depth-independent image Jacobian matrix $\hat{A}^T(y(t),q(t))$ can be computed by the estimate value of the position of the feature point in the base frame ${}^b\hat{x}(t)$. The second item in the right side represents depth compensation, and the estimate value $\hat{b}^T(q(t))$ also can be computed by the estimate value ${}^b\hat{x}(t)$.

In Eq. (22), if the true values $A^T(y(t),q(t))$ and $b^T(q(t))$ take the place of the estimate values $\hat{A}^T(y(t),q(t))$ and $\hat{b}^T(q(t))$, the closed loop kinematic equation of the soft robotic manipulator can be rewritten as:

$$\begin{aligned}\dot{q}(t) = &-J^T(q(t))A^T(y(t),q(t))K_1\Delta y(t)\\ &-\frac{1}{2}J^T(q(t))b^T(q(t))\Delta y^T(t)K_1\Delta y(t) + Y(y(t),q(t))\Delta^b x(t)\end{aligned} \tag{23}$$

where $\Delta^b x(t)\left(= {}^b\hat{x}(t) - {}^b x\right)$ indicates the 3D position error of the feature point in the base frame, and $Y(y(t),q(t))$ is a regression matrix independent of unknown position ${}^b x$. The concrete form of $Y(y(t),q(t))\Delta^b x(t)$ can be described as:

$$\begin{aligned}&Y(y(t),q(t))\Delta^b x(t)\\ &= J^T(q(t))\left\{A^T(y(t),q(t)) - \hat{A}^T(y(t),q(t))\right\}K_1\Delta y(t)\\ &+\frac{1}{2}J^T(q(t))\left\{b^T(q(t)) - \hat{b}^T(q(t))\right\}\Delta y^T(t)K_1\Delta y(t)\end{aligned} \tag{24}$$

An adaptive algorithm is designed to estimate the unknown position ${}^b x$ online:

$${}^b\dot{\hat{x}}(t) = -\Gamma^{-1}Y^T(y(t),q(t))\dot{q}(t) \tag{25}$$

where Γ is a positive-definite gain matrix.

C. Stability Analysis

Applying the image-based visual servo controller in Eq. (22) and adaptive algorithm in Eq. (25), it can be proved that the position error of the feature point on the image plane will be convergent to zero when time approaches to the infinity using the Lyapunov theory, which can be written as:

$$\lim_{t\to\infty}\Delta y(t) = 0 \tag{26}$$

To prove the conclusion above, a Lyapunov-like function is defined as follows:

$$V(t) = \frac{1}{2}\Delta y^T(t)K_1 z(q(t))\Delta y(t) + \frac{1}{2}\Delta^b x^T(t)\Gamma\Delta^b x(t) \tag{27}$$

In Eq. (27), the depth $z(q(t))$ is always positive whenever the feature point in the field of view, and it is obvious that the Lyapunov function $V(t)$ is always more than or equal to zero. Differentiate Eq. (27) leads to

$$\begin{aligned}\dot{V}(t) &= \Delta\dot{y}^T(t)K_1 z(q(t))\Delta y(t) + \frac{1}{2}\dot{z}(q(t))\Delta y^T(t)K_1\Delta y(t) + \Delta^b x^T(t)\Gamma\Delta^b\dot{x}(t)\\ &= -\Delta y^T(t)\hat{D}^T(y(t),q(t))JK_1^2J^T D(y(t),q(t))\Delta y(t) + \Delta^b x^T(t)\Gamma\Delta^b\dot{x}(t)\\ &= -\Delta y^T(t)\hat{D}^T(y(t),q(t))JK_1^2J^T\left\{D(y(t),q(t)) - \hat{D}(y(t),q(t))\right\}\Delta y(t)\\ &\quad -\Delta y^T(t)\hat{D}^T(y(t),q(t))JK_1^2J^T\hat{D}(y(t),q(t))\Delta y(t) + \Delta^b x^T(t)\Gamma\Delta^b\dot{x}(t)\end{aligned} \tag{28}$$

where

$$D(y(t),q(t)) = A^T(y(t),q(t)) + \frac{1}{2}b^T(q(t))\Delta y^T(t) \tag{29}$$

It should be noted that

$$\begin{aligned}&\Delta^b x^T(t)\Gamma\Delta^b\dot{x}(t)\\ &= \Delta y^T(t)\hat{D}^T(y(t),q(t))JK_1^2J^T\left\{D(y(t),q(t)) - \hat{D}(y(t),q(t))\right\}\Delta y(t)\end{aligned} \tag{30}$$

From Eq. (28) and Eq. (30), we can easily obtain

$$\dot{V}(t) = -\Delta y^T(t)\hat{D}^T(y(t),q(t))JK_1^2J^T\hat{D}(y(t),q(t))\Delta y(t) \tag{31}$$

Notice that $\dot{V}(t)\le 0$, therefore the Lyapunov function $V(t)$ is bounded. From Eq. (27), bounded $V(t)$ implies boundedness of the image error Δy and the estimation error of the position of the feature point $\Delta^b x(t)$. From Eq. (23), $\dot{q}(t)$ is also bounded. Similar we can conclude $\ddot{V}(t)$ is also bounded and hence $\dot{V}(t)$ is uniformly continuous. From Babarrat's Lemma, we can conclude the following convergence:

$$\lim_{t\to\infty}J^T\hat{D}(y(t),q(t))\Delta y(t) = 0 \tag{32}$$

Using a similar proof to [18], it is possible to prove that the matrix $\hat{D}(y(t),q(t))$ in the above equation has a rank of 2. From Eq. (32), as long as the soft robotic manipulator is not at singular configurations, in the invariant set the image error Δy must be equal to zero.In consequence, the image error will be converged to zero when time approaches to the infinity.

V. Experiments

To validate the adaptive image-based visual servoing above, we have conducted experiments on the soft robotic manipulator in Fig.7. The intrinsic parameters and extrinsic parameters of the endoscope camera are measure as:

$$\Omega = \begin{bmatrix}857.238 & 0 & 406.153 & 0\\ 0 & 846.798 & 304.939 & 0\\ 0 & 0 & 0 & 1\end{bmatrix}$$

$${}^cT_e = \begin{bmatrix}0 & -1 & 0 & 0\\ 1 & 0 & 0 & 0\\ 0 & 0 & 1 & 0\\ 0 & 0 & 0 & 1\end{bmatrix}$$

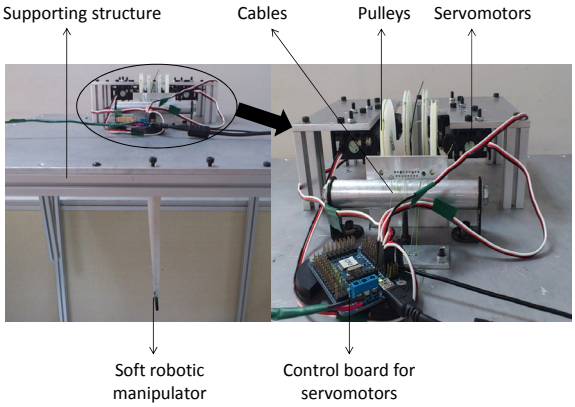

Fig.7 The soft robotic manipulator system.

The initial coordinates of the feature point on the image plane is $y(0) = (215 \quad 184)^T$ (pixels), and the desired one is $y_d = (50 \quad 150)^T$ (pixels). The control gains selected are: $K_1 = 0.001$ and $\Gamma = 10$. The initial estimated 3-D position of the feature point with respect to the base frame is ${}^b x(0) = (1.0 \quad 0.1 \quad 620.0)^T$ mm.

Fig.8 plots the trajectory of the feature point on the image plane and Fig.9 shows the image errors between current position and desired position. The results confirmed the image errors can be asymptotic converged.

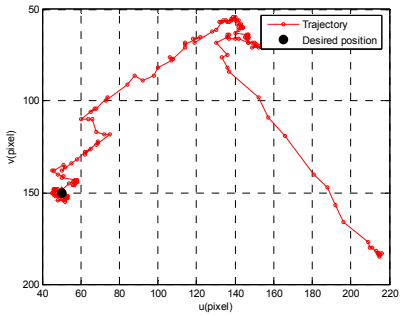

Fig.8 The trajectory of the feature point on the image plane.

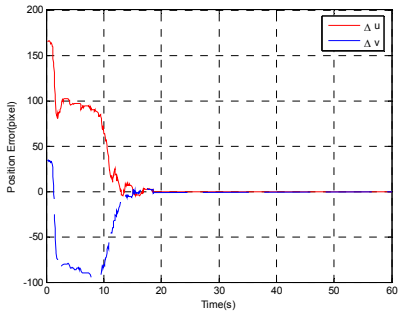

Fig.9 The image errors between current position and desired position.

VI. Conclusion

In this paper, we present a kinematic model of the soft robotic manipulator with the concept of piecewise constant curvature and designed an adaptive controller for image-based visual servoing to control the end-effector of the soft robotic manipulator to the desired position. Compare to traditional manipulators, our soft robotic manipulator is totally made of soft material, and its higher safety and dexterity make it suitable for some special applications that rigid-link manipulators cannot be applied. Motion control can be achieved using adaptive image-based visual servoing method. Results of the experiences also validate that the image-based visual servoing controller adopted in the paper could guarantee the image errors to be asymptotic converged. Future work includes application in medical surgery and complex environments exploration.

References

[1] G. Robinson and J. Davies, "Continuum robots—A state of the art," in IEEE Int. Conf. on Robotics and Automation, pp. 2849–2854, 1999.

[2] D. Trivedi, C. D. Rahn, W. M. Kier, and I. D. Walker, "Soft robotics: Biological inspiration, state of the art, and future research," Applied Bionics and Biomechanics, vol. 5, no. 3, pp. 99–117, 2008.

[3] R.Cieslak and A. Morecki, "Elephant trunk type elastic manipulator – A tool for bulk and liquid type materials transportation," Robotica, vol.17, pp. 11–16, 1999.

[4] M. Hannan and I. D. Walker, "Kinematics and the implementation of an elephant's trunk manipulator and other continuum style robots," J. Robot. Syst., vol. 20, pp. 45–63, 2003.

[5] R. Pfeifer, M. Lungarella, and F. Iida, "Self-organization, embodiment, and biologically inspired robotics," Science, vol. 318, pp. 1088–1093, 2007.

[6] M. Cianchetti, A. Arienti, M. Follador, B. Mazzolai, P. Dario, and C. Laschi, "Design concept and validation of a robotic arm inspired by the octopus," Materials Science and Engineering C, vol. 31, pp. 1230–1239, 2011.

[7] Wolf, H. B. Brown, R. Casciola, A. Costa, M. Schwerin, E. Shamas and H. Choset, "A mobile hyper redundant mechanism for search and rescue tasks," Proc. IEEE/RSJ Intl. Conf. on Intelligent Robots and Systems, Taipei, Taiwan, pp. 2889–2895, 2003..

[8] N. Simaan, R. Taylor and P. Flint, "A dexterous system for laryngeal surgery", IEEE Conf. Robotics and Automation, New Orleans, pp. 351–357, 2004.

[9] G. Chen, M. T. Pham and T. Redarce, "Sensor-based Guidance Control of A Continuum Robot for A Semi-autonomous Colonoscopy," Robotics and Autonomous Systems, vol. 57, no. 6, pp. 712-722, 2009.

[10] W. Hannan and D. Walker, "Kinematics and the implementation of an elephant's trunk manipulator and other continuum style robots," Journal of Robotic Systems, vol. 20, no. 2, pp. 45–63, Feb 2003.

[11] R. J. Webster, B. A. Jones, "Design and Kinematic Modeling of Constant Curvature Continuum Robots: A Review," International Journal of Robotics Research, vol. 29, no. 13, pp. 1661-1683, 2010.

[12] S. Haddadin, A. Albu-Schaffer, and G. Hirzinger, "Requirements for Safe Robots: Measurements, Analysis and New Insights," The International Journal of Robotics Research, vol. 28, no. 11-12, pp.1507–1527, 2009.

[13] T. Zheng, D. T. Branson, E. Guglielmino, and D. G. Caldwell, "A 3D Dynamic Model for Continuum Robots Inspired by An Octopus Arm," in IEEE Int. Conf. on Robotics and Automation, pp. 3652–3657, 2011.

[14] D.B. Camarillo, C.F. Milne, C.R. Carlson, M.R. Zinn, J.K. Salisbury, "Mechanics modeling of tendon-driven continuum manipulators", IEEE Trans. Robot. vol. 24, no. 5, pp.1262–1273, 2008

[15] G. Hu, W. Mackunis, N. Gans, W. E. Dixon, J. Chen, A. Behal, D.M. Dawson, "Homography-Based Visual Servo Control with Imperfect Camera Calibration," IEEE Transactions on Automatic Control, vol. 54, no. 6, pp. 1318-1324, 2009.

[16] Y. H. Liu, H. Wang, C. Wang and K. Lam, "Uncalibrated visual servoing of robots using a depth-Independent interaction matrix," IEEE Trans. on Robotics, vol. 22, no. 4, pp.804-817, 2006.

[17] H. Wang, Y. H. Liu and D. Zhou, "Adaptive visual servoing using point and line features with an uncalibrated eye-in-hand camera," IEEE Trans. on Robotics, vol. 24, no. 4, pp. 843-857, 2008.

[18] Y. H. Liu and H. Wang, "An adaptive controller for image-based visual servoing of robot manipulators," The 8th World Congress on Intelligent Control and Automation, pp. 988-993, 2010.